

Quantifying preferential flows on two farmlands in the North China plain using dual infiltration and dye tracer methods

Jie Zhang ^a, Quan Sun ^{a,b}, Na Wen ^a, Robert Horton ^c, Gang Liu ^{a,*}

^a Department of Land Use Engineering, College of Land Science and Technology, China Agricultural University, Beijing 100193, China

^b Bureau of Agriculture and Rural Affairs of Nanning Municipality, Nanning 530000, China

^c Department of Agronomy, Iowa State University, Ames, IA 50011, USA

ARTICLE INFO

Handling Editor: Haly Neely

Keywords:

Preferential flow
Matrix infiltration
DI method
Dye tracer method
Wormholes

ABSTRACT

Preferential flow, as a significant part of soil water infiltration, affects crop water use efficiency and pollutant transport in soil. Although it is important to properly assess the effect of preferential flow on soil water infiltration, there is a lack of widely accepted methods to quantify preferential flow. In this study, a new dual infiltration method (DI method) was used to quantify the contribution of preferential flow at two farmlands in the North China plain. The experiments were performed at two field sites (LY and SZ). To apply the new method, a double-ring infiltrometer was used to measure the steady-state infiltration rate (i.e., when infiltration rate becomes constant or stable with time, SIR) at the field sites, while a constant-head infiltrometer was used to measure the saturated hydraulic conductivity of packed soil columns consisting of disturbed soil obtained from each field site. Water flow in the disturbed soil columns was used to approximate the matrix infiltration rate (MIR), and the difference between SIR and MIR represented the preferential flow infiltration rate (PFIR). A dye tracer was also applied to the infiltrometers to quantify the proportion of preferential flow. For the LY site, the DI method found that the PFIR was 68 times larger than the MIR, while, based on the dye tracer method, the PFIR was only 2 times larger than the MIR. The DI and dye tracer method derived values of PFIR were similar for the SZ site, with MIR accounting for 61% (DI method) and 67% (dye tracer method) of the SIR. Wormholes were an important factor in the preferential flow generated in the LY site. The total areas of wormholes visible at the surface and the PFIR values were significantly positively correlated, $r = 0.79$ ($P < 0.05$). The DI method reasonably quantified preferential flow at the field sites, while the dye tracer method might underestimate preferential flow in soil with abundant macropores.

1. Introduction

Preferential flow, a prevalent problem in farmlands, refers to the rapid movement of water through pathways such as fissures and tubular pores formed by earthworms and decaying roots. Due to the presence of preferential flow, the contact time between solute (e.g., phosphorus) and soil matrix is reduced, making it difficult for solutes to be adsorbed and more likely to cause problems such as nutrient loss (Grant et al., 2019; Kianpoor Kalkhajeh et al., 2021). In addition, the presence of preferential flow channels affects the occurrence of surface runoff, thus affecting the hydrological cycle, soil erosion, agricultural production, and various biochemical processes within the vadose zone (Stewart et al., 2015); and it can accelerate the contaminant transport rate, which in turn affects the quality of groundwater (Guo and Lin, 2018).

It is important to improve the understanding of preferential flow in soils to reduce nutrient loss and protect groundwater resources (Salvador et al., 2011). Dye tracer methods (Sander and Gerke, 2007; Alaoui and Goetz, 2008; Kodešová et al., 2012; Laine-Kaulio et al., 2015; Filipović et al., 2020), lysimeter tracer studies (Greve et al., 2010), ponded and tension infiltrometer measurements (Ankeny et al., 1991; Mohanty et al., 1996) and a liquid latex method (Abou Najm et al., 2010) have been used to assess preferential flow. Dye tracer methods (Flury and Flühler, 1995) are used to visualize preferential flow pathways, and image processing techniques are used to analyze the relationship between preferential flow infiltration and steady-state infiltration. Tobella et al. (2014) used the dye tracer method to investigate the influence of trees on soil permeability and preferential flow. However, the dye tracer method requires destructive sampling and is influenced by soil cohesion,

* Corresponding author.

E-mail address: liug@cau.edu.cn (G. Liu).

which may not reveal all the preferential flow channels (Beven and Germann, 2013). Greve et al. (2010) and Stumpf and Maloszewski (2010) used a lysimeter combined with a tracer to study water movement through the soil matrix and the preferential flow channels. This method assumed equal isotopic content in the water passing through the preferential flow channel as well as in precipitation, which is prone to measurement error during long experiments. Sanders et al. (2012) used liquid latex to seal visible preferential flow channels on field surfaces to prevent the occurrence of preferential flow and force water through the soil matrix, thereby separating the contribution of preferential flow from matrix flow. However, this method only sealed visible shrinkage cracks and bio-pores and could not eliminate the contribution of structural pores to preferential flow. Zhang et al. (2019a) proposed a method to quantitatively partition preferential flow and matrix infiltration in forest soils, which measured matrix infiltration by using fine sand to shelter the preferential flow paths. While the method has good performance in forest soils, its accuracy in farming soils needs further validation. Meanwhile, the operation of sheltering the soil surface with fine sand and nylon cloth will affect water infiltration into soils, especially soil with high sand content. There is a need for a simple method to identify preferential soil water flow.

The double-ring infiltrometer is a standard method for measuring in-situ water infiltration (Khodaverdiloo et al., 2017; Zhang et al., 2017). It can measure water infiltration rate in fields with macropores. Benegas et al. (2014) assessed the effect of the presence of trees on pasture permeability by using a double-ring infiltrometer. Zhang et al. (2019a) also used a double-ring infiltrometer to measure water infiltration. Moreover, Wu et al. (2021) used the device to assess soil water recharge in response to root decay. And, the constant-head infiltrometer is a common method for measuring the saturated hydraulic conductivity which can be used for medium- and even fine-textured soils (e.g., well-structured Bt horizons) (Klute and Dirksen, 1986; Wu et al., 1997; Zeleke

and Si, 2005; van Schaik et al., 2010; Mei et al., 2018).

The combination of a field-based double-ring infiltrometer with a laboratory-based constant-head infiltrometer (defined as a dual infiltration method, or DI method) may provide a new solution for the quantification of preferential flow. Although there is no literature to support the calculation of preferential flow by using the so-called DI method, the underlying physics mechanism for this method is rather clear and reasonable. Because the field measurements are conducted at field sites with preferential flow paths, while the laboratory measurements are conducted using disturbed soil columns without macropore or preferential flow structure (forcing water to move only in the soil matrix). The difference between the measured water flow rates by the two methods is assumed as the preferential flow related infiltration rate. For the DI method, when repacking and measuring water flow rate, we are destroying both the preferential flow path and the structure of the soil. According to the definition of macropore (pores average diameter greater than 60 μm) (Arrington et al., 2013), for sandy soil (pores average diameter greater than 50 μm) (Marshall et al., 1996), the percentage of soil structure that is not responsible for preferential flow is negligibly small. Therefore, the preferential flow infiltration rate derived from the DI method is plausible, at least for sandy soil.

The main objective of this study was to quantify the contribution of preferential flow using the DI method and dye tracer method in farmland with different soil types. By comparing the experimental results, we also analyzed the performance of the two methods.

2. Materials and methods

2.1. Study areas

Experiments were performed at the Lvyuan research station (LY, 39°57'N, 116°18'E) and the Shangzhuang research station (SZ, 40°08'N,

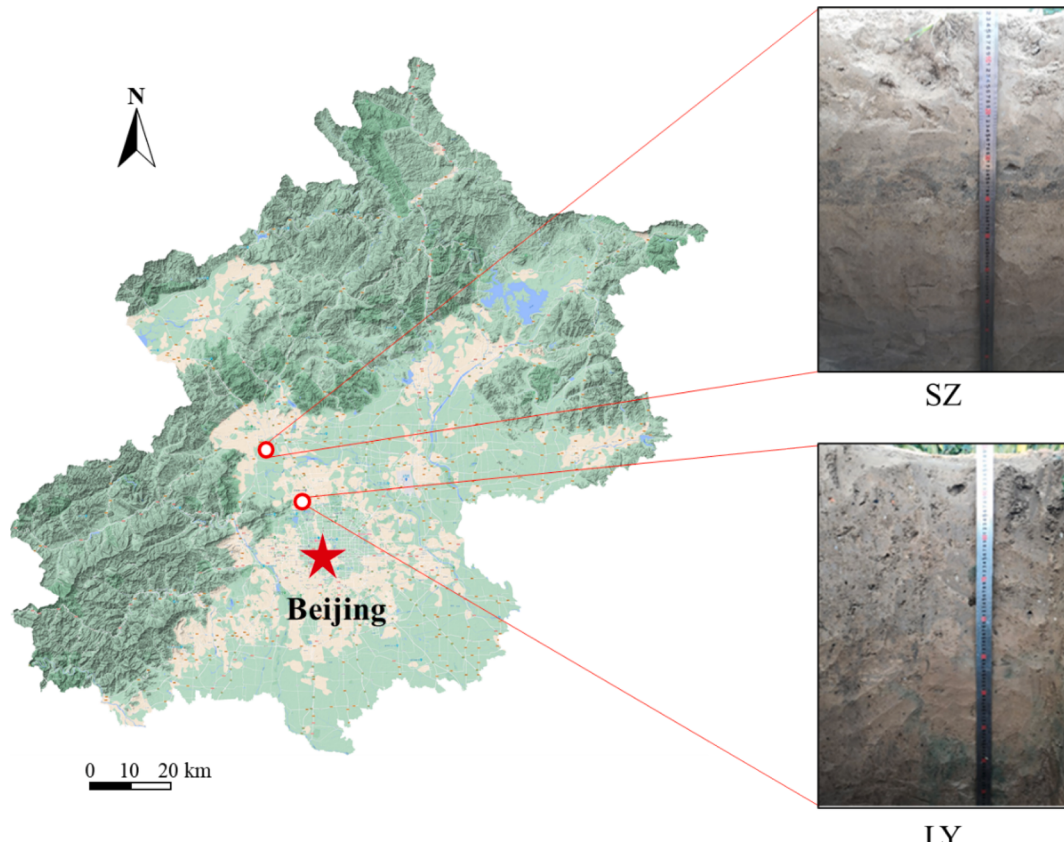


Fig. 1. Detail locations and corresponding soil profiles of the two sites (LY and SZ).

116°10'E), which are approximately 15 km away from each other (Fig. 1). Both sites are located in the North China piedmont impingement plain, with a warm-temperate semi-humid continental monsoon climate zone. The LY site was traditional farmland that had been continuously no-till for 13 years. Spring maize and Chinese cabbage are planted without mulch all year round at the LY site. The mean annual temperature is 11.5 °C, and the mean annual precipitation is 640 mm, mainly from June to August. The organic matter content of the soil is 10.5 g kg⁻¹, and the soil type is meadow brown with a silt loam texture. The SZ site was on a long-term locational experiment station under traditional rotary tillage for over 15 years and the last tillage was three months prior to the initiation of this study. Rainfed sweet potatoes and winter wheat are planted at the SZ site. Its climatic conditions are similar to the LY site, and the soils have an organic matter content of 6.4 g kg⁻¹.

2.2. DI method

2.2.1. Method introduction

Germann and Beven (1985) suggested that soil water movement with macropores consists of two main components. One is matrix infiltration, which is controlled by capillary activity. The other is preferential flow infiltration, in which soil water flows only under the influence of gravity. Infiltration can be expressed by

$$i = i_p + i_m \quad (1)$$

where i is the steady-state infiltration rate (i.e., the sum of the infiltrations rates through pores in the soil matrix and macropores, STR), LT⁻¹; i_m is the matrix infiltration rate (MIR), LT⁻¹; i_p is the preferential flow infiltration rate (PFIR), LT⁻¹. In this study, we presented a new DI method. For this method, a field-based double-ring infiltrometer combined with a laboratory-based constant-head infiltrometer was used to determine the steady-state infiltration rate and the matrix infiltration rate of test sites.

2.2.2. SIR measurement

A specially designed automatic double-ring infiltrometer was used to measure SIR (Sun et al., 2020). The detailed construction of the automatic double-ring infiltrometer can be seen in Fig. 2. The diameters of the inner and outer rings of this double-ring infiltrometer were 17.6 cm and 30 cm, respectively (Bagarello et al., 2009; Stewart et al., 2015; Stewart et al., 2016). Where the laser rangefinder was used to measure and record the water level changes of the water supply container; the

water level controller and solenoid valve were used to control the water level in the double-ring and keep the head constant.

Infiltration measurements were performed at nine randomly selected locations at each field station. All measurement locations in the LY site had wormholes visible at the soil surface. In this study, SIR was measured simultaneously with the dye tracer experiment, which will be described in detail. During the experiment, the two rings were inserted into the soil at 5 cm depth, and the water level was maintained at 5 cm in the inner and outer rings. We recorded the cumulative infiltration volume from the beginning of the experiment, and the infiltration time for each location was not less than 60 min until the infiltration rate reached stability. Finally, we used OriginPro 2021b (Moberly et al., 2018) to fit the cumulative infiltration volume versus time data with the Philip infiltration (Philip, 1957) (see Fig. 3 for details)

$$I(t) = Bt + St^{0.5} \quad (2)$$

where $I(t)$ is the cumulative infiltration, L; t is the time, T; S is the sorptivity value, LT^{-0.5}; B is a steady infiltration rate, LT⁻¹.

The infiltration rate was calculated from $i(t) = \frac{dI(t)}{dt}$

$$i(t) = 0.5St^{0.5} + B \quad (3)$$

where $i(t)$ is the soil water infiltration rate, LT⁻¹. In Philip's model (Eq. (2)), after the initial infiltration stage, the $I(t) \sim t$ curve is approaching a linear trend ($i(t)$ can be approximated as the constant B , and the first term of Eq. (3) is relatively small, compared with the value of B), as will be illustrated by our results presented in Fig. 3. Therefore, when t is large enough, the infiltration can be regarded as the steady state approximation, which significantly simplified the procedure for obtaining SIR.

2.2.3. MIR measurement

The MIR values were measured by a laboratory constant-head infiltrometer (Bouwer, 1986; Klute and Dirksen, 1986). The device was assembled from a Mariotte bottle, an acrylic tube (R = 3.25 cm), an iron stand, and a plastic funnel. We measured the saturated hydraulic conductivity of the surface soil (0–20 cm) at nine locations (within a square of 5 by 5 m) to determine the spatial variability in two sites (LY and SZ). We assumed that spatial heterogeneity could be neglected in the two sites. So, only one location within the square was selected for each test site to measure the MIR.

Soil samples were taken at 5 cm intervals and to a depth of 95 cm. The particle size distribution and the bulk density of soils were also

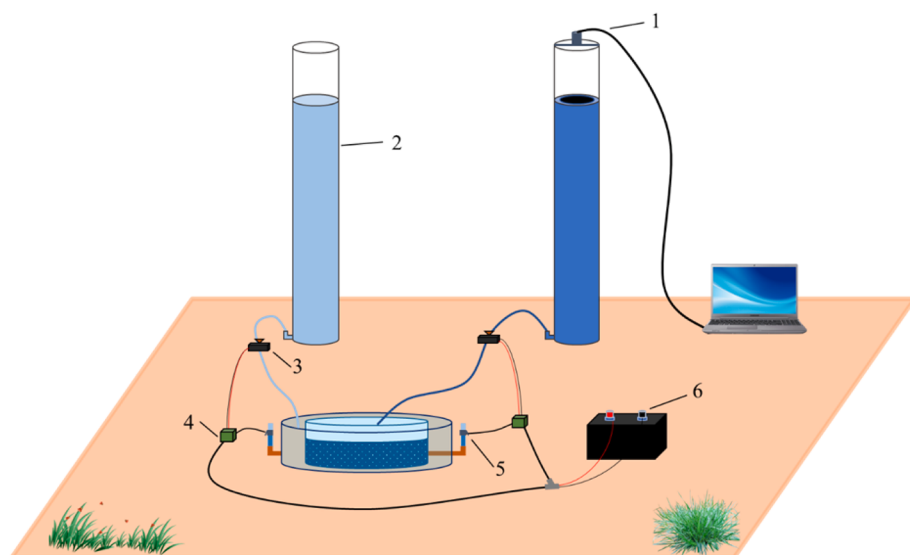


Fig. 2. Schematic diagram of the automatic double-ring infiltrometer. 1, laser distance sensor; 2, water supply container; 3, solenoid valve; 4&5, non-contact water level controller; 6, battery.

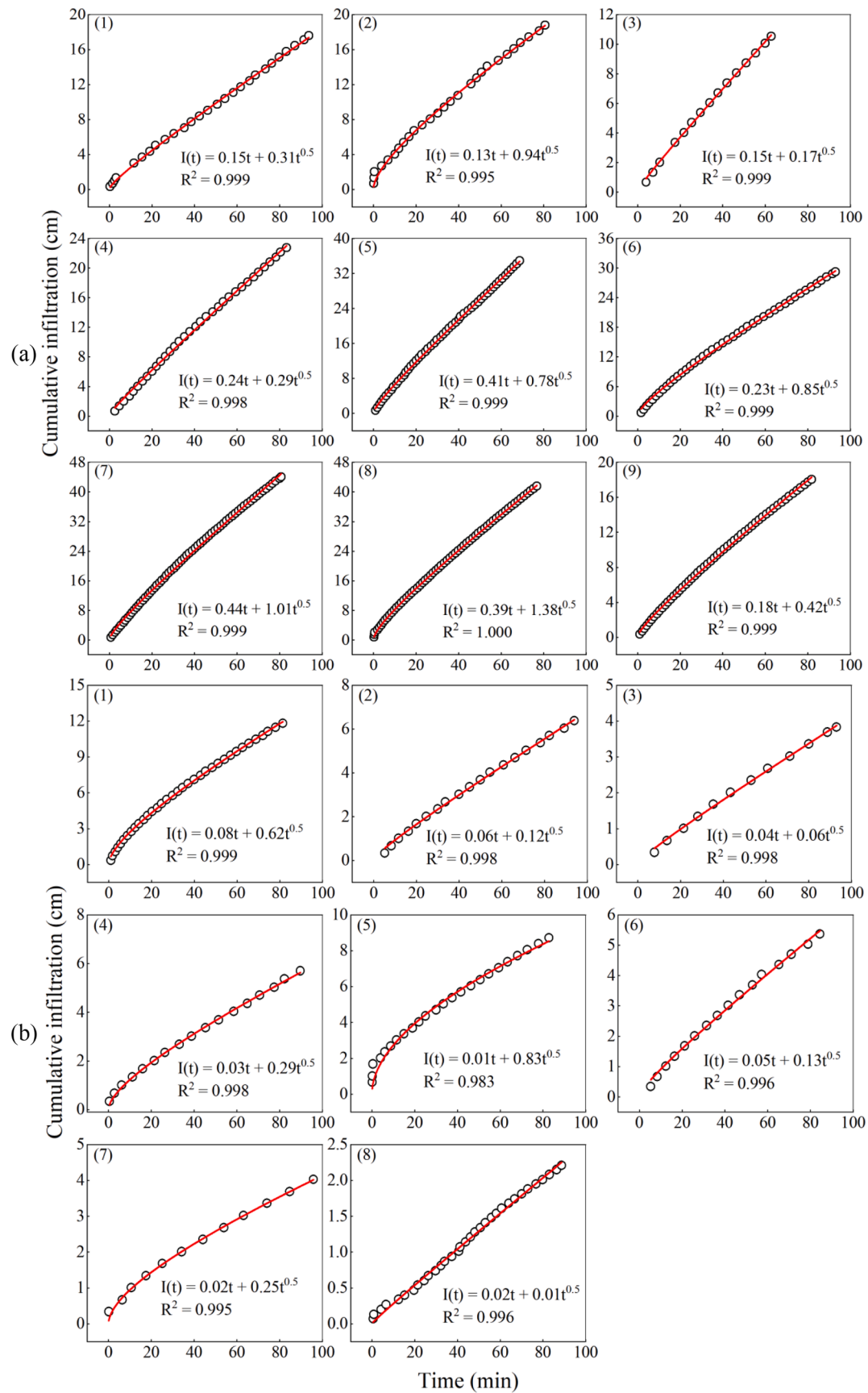


Fig. 3. The changes of cumulative infiltration with time at different locations of the LY site (a) and SZ site (b), respectively.

measured by the laser diffraction method (Svensson et al., 2022) and the core cutter method (Grossman and Reinsch, 2002), respectively (Table 1). Soil samples were dried and ground, then passed through a 2 mm sieve to remove larger stone particles, grassroots, and other impurities. Then we repacked with sieved soil material into a 5 cm high column in two parts according to the soil bulk density of the sampling locations and finally measured the saturated hydraulic conductivity. During the measurement, the height of the Mariotte bottle was adjusted to keep the ponded water head at 3 cm. After the soil column was saturated for 12 h, we started recording the outflow volume each hour. When three consecutive water outflow volumes were similar, we stopped the measurement and calculated the average of the three. The saturated hydraulic conductivity of the soil column was calculated by

$$K_s = \frac{Q}{At} \frac{L}{\Delta H} \quad (4)$$

where K_s is the saturated hydraulic conductivity, LT^{-1} ; Q is the volume of outflow, L^3 ; A is the cross-sectional area of the soil column, L^2 ; t is the time interval (during which outflow is collected), T ; L is the height of the soil column, L ; and ΔH is the head difference between the two ends of the soil column, L . Finally, the effective vertical saturated hydraulic conductivity (Shukla, 2013) of the soil within the wetted volume under the infiltrometers was calculated by

$$K_{eff} = n / (1/K_1 + 1/K_2 + 1/K_3 + \dots + 1/K_n) \quad (5)$$

where the height of the soil cores was 5 cm, and K_1, K_2, \dots, K_n were the measured saturated hydraulic conductivity of the 5-cm long cores, and n was the number of 5-cm intervals (12 for LY and 4 for SZ sites). We determined the soil water profile by measuring soil water content in 5-cm depth increments from the surface to 95 cm depth for the two sites. And, we also determined the soil water profile by the depth of the stained area, which was 60 (LY) and 20 cm (SZ). Since the dye gets adsorbed on the soil particles, this caused the wetting front to be ahead of the stained front. However, the difference between the two fronts was less than 5 cm in our study. Therefore, for convenience, we chose the stained profile to determine the soil moisture profile.

2.3. Dye tracer method

2.3.1. Methods introduction

The dye tracer experiment was carried out simultaneously with the determination of SIR. During the experiment, Brilliant Blue FCF (C.I.

Table 1
Soil physical properties of the two experimental sites (LY and SZ).

Depth (cm)	LY					SZ				
	sand	silt %	clay	ρ_b g cm ⁻³	e	sand	silt %	clay	ρ_b g cm ⁻³	e
0–5	47.9	48.9	3.2	1.33	0.50	78.5	19.1	2.4	1.46	0.45
5–10	49.2	47.7	3.1	1.30	0.51	80.1	17.9	2.1	1.48	0.44
10–15	47.6	49.0	3.3	1.25	0.53	80.9	17.2	2.0	1.49	0.44
15–20	44.6	53.7	1.6	1.13	0.57	81.0	17.0	2.0	1.60	0.40
20–25	48.8	48.1	3.1	1.29	0.51	81.0	17.0	2.0	1.58	0.40
25–30	45.2	51.7	3.2	1.48	0.44	82.7	15.4	1.8	1.65	0.38
30–35	43.2	53.0	3.8	1.55	0.42	65.4	30.8	3.8	1.68	0.37
35–40	42.6	53.7	3.8	1.54	0.42	85.6	12.8	1.6	1.63	0.39
40–45	37.7	58.2	4.1	1.52	0.43	92.3	6.7	1.0	1.50	0.43
45–50	37.6	57.9	4.5	1.54	0.42	91.8	7.1	1.2	1.54	0.42
50–55	33.5	61.7	4.9	1.43	0.46	90.2	8.3	1.5	1.51	0.43
55–60	28.5	64.8	6.6	1.57	0.41	92.3	6.3	1.4	1.51	0.43
60–65	37.4	58.1	4.4	1.46	0.45	93.7	4.9	1.4	1.51	0.43
65–70	31.3	63.8	5.0	1.49	0.44	92.0	6.8	1.2	1.50	0.43
70–75	63.4	35.9	0.7	1.49	0.44	92.4	6.2	1.3	1.51	0.43
75–80	33.4	63.8	2.9	1.57	0.41	83.5	14.5	2.0	1.54	0.42
80–85	35.3	59.4	5.3	1.54	0.42	92.8	5.8	1.3	1.53	0.42
85–90	36.7	58.8	4.5	1.54	0.42	87.3	11.1	1.6	1.53	0.42
90–95	29.7	65.7	4.7	1.51	0.43	91.6	7.2	1.3	1.51	0.43

* e is the total porosity.

42090, supplied by Tianjin Duofuyuan Industrial Co., Ltd, China) dye solution of 4 g L⁻¹ concentration was chosen as a tracer for the preferential flow paths (Flury and Flühler, 1995). We added the dye solution and water to two water supply containers, which were then supplied to the inner and outer rings, respectively. The dye application was more than 60 min at each test location. 24 h after completing the dye application, the middle profile (i.e., the vertical plane going through the center of the infiltrometer) was excavated for assessing the distribution of the dyed area under the infiltrometer (see Fig. 4a for details). Finally, a ruler was placed next to the soil profile for image processing, and the photographs (resolution: 2736 × 3648 pixels) of the stained profile were taken.

The stained areas of the soil profile under the infiltrometers were used to quantify the contribution of preferential flow according to (van Schaik, 2009)

$$PF_{fr} = 1 - \frac{MID \times W}{A_{ts}} \quad (6)$$

where PF_{fr} is the proportion of preferential flow in the whole infiltration process; MID is the depth of matrix infiltration, which refers to the depth when the stained area of soil profile accounts for not less than 80%, L ; A_{ts} is the total stained area of the soil profile, L^2 ; W is the width of the soil profile, and it is equal to the diameter of the inner ring (17.6 cm). When the stained area of the images exceeded 80% of the total area, all the stained area was considered to be matrix infiltration (MI); if not, it was preferential flow infiltration (PFI) (Benegas et al., 2014; Mei et al., 2018). The proportion of PFI can be calculated by

$$PF_{fr} = \frac{PF_{Ar1} + PF_{Ar2} + \dots + PF_{Ari}}{A_{ts}} \quad (7)$$

where PF_{Ari} is the stained area of the image identified as PFI, L^2 .

In this dye tracer experiment, the stained area of the intermediate profile (Fig. 4a) was used to represent the stained volume of each test site. The photographs of the stained profiles were corrected and cropped by Photoshop CC 2019 (Adobe Systems, Inc., San Jose, California, US), and then the stained area of each photograph was counted by ImageJ (National Institutes of Health, US) (Ferreira and Rasband, 2012).

2.3.2. Digitizing process of the stained photographs

(1) Geometric correction and cropping

Due to the unfixed shooting angle, some of the stained soil profile photographs may have been deformed. Therefore, the Perspective

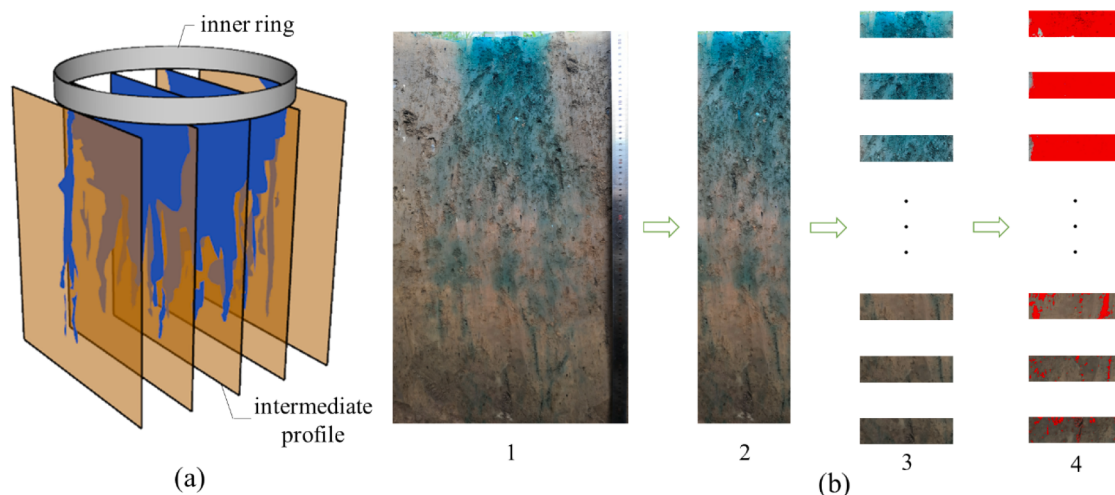


Fig. 4. Schematic diagram of stained soil profiles and photograph processing. (a) Schematic diagram of stained soil profile excavation, the intermediate profile was selected to count the stained area in this study. (b) Digitizing process of stained profile photographs: the original photograph was corrected using PS (b1), cropped to a suitable width according to the size of the inner ring (b2), cropped to 5 cm high for ease of calculation (b3), and the stained area was counted using ImageJ (the red parts) (b4). (For interpretation of the references to color in this figure legend, the reader is referred to the web version of this article.)

Cropping tool of Photoshop was used to correct the obtained photographs according to the vertical ruler in the images (Fig. 4-b1), while cropping off the non-infiltrated areas (Fig. 4-b2) (Alaoui and Goetz, 2008; Wang et al., 2018a). For statistical convenience, we also cropped corrected photographs into small images of 5 cm in height (Fig. 4-b3).

(2) Stained area statistics

We used ImageJ to count the stained area of cropped images (resolution: 1276×363 pixels) following the procedures outlined by the manual for ImageJ. We transformed the cropped images into RGB color mode and then separated the image into stained and non-stained areas by the thresholding method. Where the reference setting values for R, G, and B were 120, 170, and 190, respectively. After saving the image ($72.5 \text{ pixels cm}^{-1}$) in TIFF format, we used the tool that comes with the ImageJ to count the stained areas (Filipović et al., 2020).

Because the color of the wormholes was significantly darker than the other areas after staining (Fig. 7), we also used ImageJ to count the diameter of open wormholes on the infiltration surface.

3. Results and discussion

3.1. Results of the DI method

The results obtained by the DI method are shown in Table 2. The MIR of each experimental station was 0.05 (LY) and 0.26 m d^{-1} (SZ). The PFIR values for the LY site calculated using Eq. (1)-(5) ranged from 1.87 to 6.36 m d^{-1} , and PFIR values were 34 to 118 times larger than the MIR values. The PFIR values ranged from 0 to 0.89 m d^{-1} in the SZ site, averaging 39% of the SIR values. The results in Table 3 showed that the horizontal spatial variabilities of K_s were 10.17% (LY) and 12.22% (SZ), which proved that it was reasonable to measure one MIR at each site. A similar assumption was also used by Surajit et al. (2006).

As Germann and Beven (1985) said, although the preferential flow channels represent only a minor fraction of the total soil mass, their contribution to flow may exceed that of the soil matrix by several orders of magnitude. The results of Zhang et al. (2019a) showed that PFIR values were 2–5 times higher than MIR values during steady infiltration. The contribution of preferential flow to total flow in their results was lower than that of our study. One possible explanation for this is that their method, which determined MIR by sheltering the preferential flow channel with fine sand, did not thoroughly exclude the contribution of

Table 2
Infiltration data at the LY and SZ sites determined by the dual infiltration method.

No.	SIR	LY MIR m d^{-1}	PFIR	PFIR/SIR %	No.	SIR	SZ MIR m d^{-1}	PFIR	PFIR/SIR %
1	2.17	0.05	2.16	98	1	1.14	0.26	0.87	77
2	1.89		1.87	97	2	0.76		0.50	65
3	2.13		2.11	97	3	0.50		0.24	47
4	3.51		3.50	98	4	0.46		0.20	42
5	5.92		5.90	99	5	0.17		0.00*	0
6	3.28		3.27	98	6	0.73		0.47	64
7	6.38		6.36	99	7	0.24		0.00*	0
8	5.56		5.54	99	8	0.33		0.07	20
9	2.55		2.53	98					
Mean			3.66	98				0.29	39
CV			45.6 %	0.7 %				96.6 %	71.8 %

* SIR, the steady-state infiltration rate; MIR, the matrix infiltration rate; PFIR, the preferential flow infiltration rate; CV, coefficient of variation.

* At test locations #5 and #7, the MIR values measured by the constant-head infiltrometer were greater than the SIR values measured by the double-ring infiltrometer. Considering the different measurement accuracies and error sources of the two instruments, we assumed that the MIR was equal to the SIR, i.e., the PFIR value was 0 m d^{-1} at the two locations in the SZ site. During the experiment, one measurement location in the SZ site was discarded due to a leak in the water supply pipe, so the SZ site had one less measurement location than the LY site.

Table 3

Saturated hydraulic conductivity of surface soil (0–20 cm) in the two experimental sites (LY and SZ).

Saturated hydraulic conductivity (m d^{-1})									Mean	CV	
	1	2	3	4	5	6	7	8	9		
LY	0.32	0.32	0.33	0.33	0.39	0.40	0.30	0.34	0.30	0.34	10.17 %
SZ	0.23	0.24	0.26	0.22	0.22	0.18	0.17	0.22	0.21	0.22	12.22 %

preferential flow, because it is well known that fine sand is commonly related to water flow instability which might trigger finger flows, another kind of preferential flow (Hill and Parlange, 1972; Wang et al., 2018b; Liu et al., 2021). In contrast, the method used in our study destroyed all preferential flow pathways. Sanders et al. (2012) reported that water outflow from macropores connected to the surface accounted for 99% of the total infiltration. In addition, Alaoui (2015) used the MACRO model to assess preferential flow in grassland and found that the proportion of water outflow from macropores to groundwater varied between 81% and 93% in brown soils. Their findings are in good agreement with the results in the LY site (97%).

Of course, there is a limitation to our method in that we assume that the only differences between disturbed and undisturbed soils are macropores. This is possible in homogeneous soil, but further validation is needed in heterogeneous soil.

3.2. Results of the dye tracer method

The results of dye tracer experiments in the two sites are shown in Fig. 5. As shown in Fig. 5a, the migration of the Brilliant Blue FCF dye solution in the soil profiles was visible (LY). In the 0–30 cm soil layer, the dye solution underwent one-dimensional vertical infiltration at most of the field test locations, and the soil profiles were stained uniformly. The characteristics of the stained profiles are similar to the results obtained by Zhu et al. (2019). Below the 30 cm soil layer, the non-stained area gradually increased, which may be related to preferential flow movement (Schwen et al., 2014; Marquart et al., 2020). The dye solution rapidly moved through the macropores, showing scattered stained patches in the soil profiles. The soil profiles were stained to depths between 60 and 100 cm. As can be seen in Fig. 5b, the stained areas of soil profiles at the SZ site were concentrated and continuous, with less preferential flow occurring. The stained depth of soil profiles at the SZ

site was approximately 15 to 25 cm, which was generally consistent with the tillage depth.

As shown in Fig. 6, the results indicated that the proportion of stained area in the soil profile became lower as the depth of the soil layer increased. The stained depth of each test site in the LY site averaged about 60 cm, while the stained depth in the SZ site was about 15 cm. The results calculated by Eqs. (6) and (7) indicated that PFI was the dominant infiltration mode in the LY site. The PFI can reach a maximum of 78% and an average of 53% of the steady-state infiltration. However, the MI dominated the flow in the SZ site. The PFIR ranged from approximately 8% to 65% of the SIR, with an average of 33% of the SIR. The results of Wu et al. (2015) demonstrated that by using the dye tracer method the percentage of preferential flow in the farmland ranged from 19.72% to 66.64% at different irrigation levels.

3.3. Comparison of dye tracer method and DI method

By comparing the results for field and laboratory measurements, we further analyzed the performance of the two methods. In the LY site, although the two methods' results both indicated that PFI was the central infiltration mode, there was a vast gap in the contribution of PFI. The results of the DI method showed that the proportion of the PFI was above 97% in all test sites, while the results of the dye tracer method showed that the average contribution of PFI was just over 50%. In contrast, for the SZ site, the results of the two methods were relatively close, with the proportion of the PFI ranging from 30% to 40%. From these results, we conjectured that the dye tracer method may underestimate the contribution of the PFI in the no-tilled field which had abundant macropores. One possible mechanism for the poor performance of the dye tracer method is that dye solution (such as Brilliant Blue FCF dye) is prone to adsorption to soil particles during infiltration, which is related to large experimental errors (Germán-Heins and Flury,

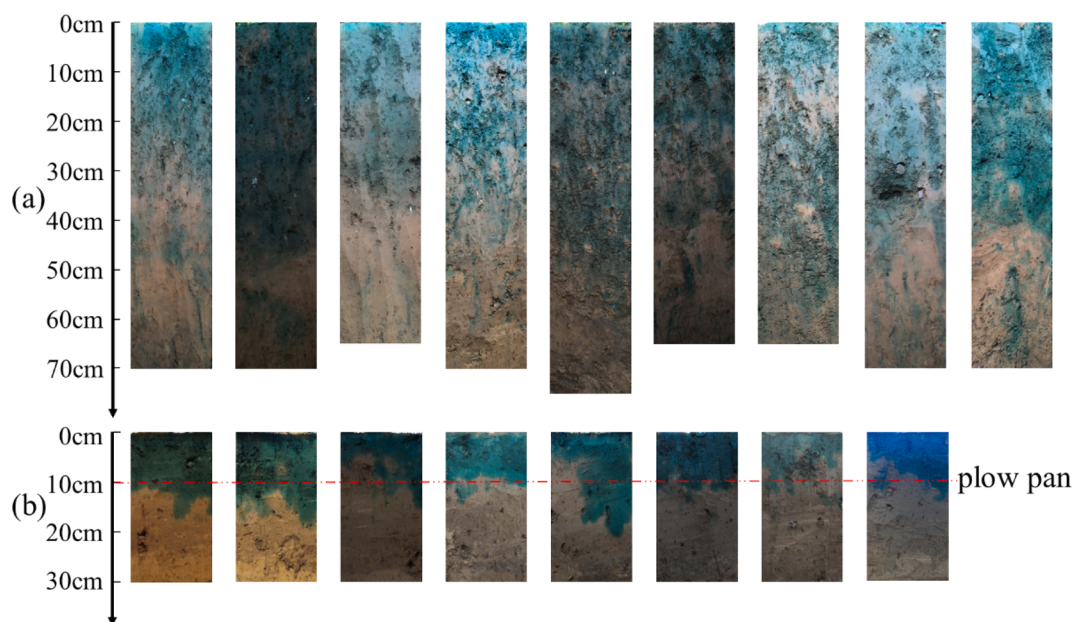


Fig. 5. Stained photographs of intermediate profiles in the LY (a) and SZ (b) sites, where the red line is the location of the plow pan. (For interpretation of the references to color in this figure legend, the reader is referred to the web version of this article.)

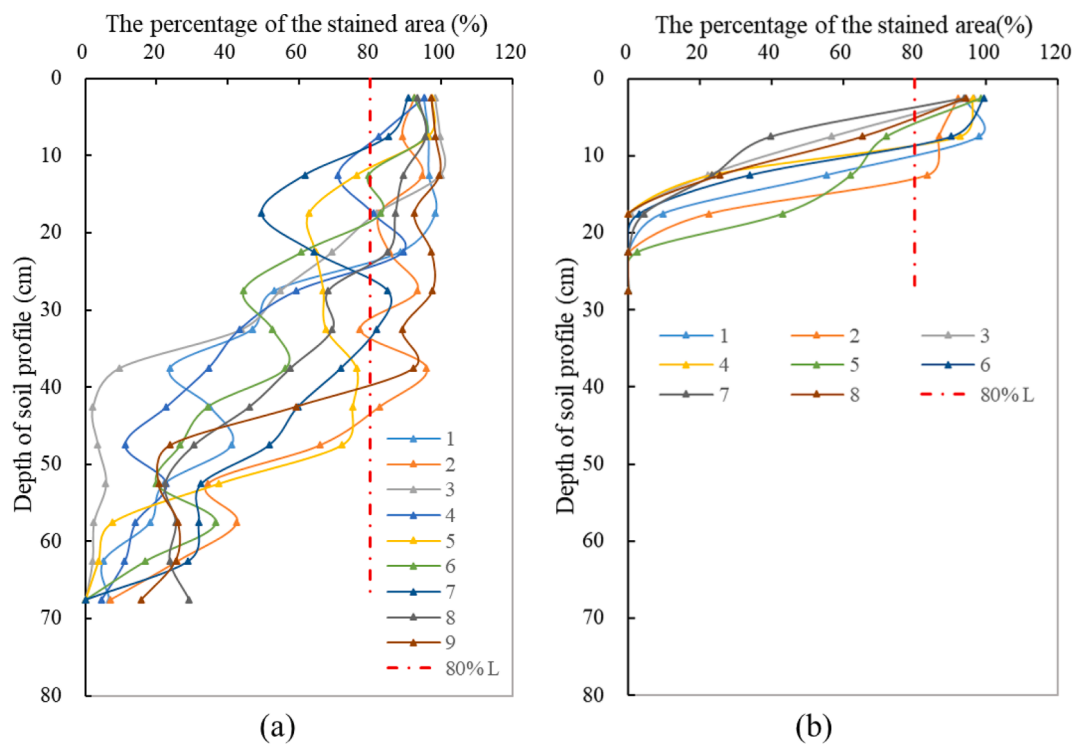


Fig. 6. The percentage of the stained area at the two experimental sites (a: LY, b: SZ), where 80% L is the dividing line between the matrix infiltration and the preferential flow infiltration.

2000). Similar underestimations were also reported by Cey and Rudolph (2009) and Nobles et al. (2010), the underestimation-related errors may derive from two main sources. The first source was the digitizing process of stained photographs. In the dye tracer method, the stained area identifies as the MI area when the stained area is not less than 80% of the total profile area. Of these, 80% is only an empirical parameter, and its applicability in fields with various tillage practices and textures is still unclear. The second source came from the experimental apparatus. Due to the irregularity of the preferential flow channels (e.g., zig-zag shaped earthworm burrows, fractal underground root system) and the small size of the automatic double-ring infiltrometer, the Brilliant Blue FCF dye solution is highly susceptible to flowing out of the experimental area as was observed by Kodešová et al. (2015). It is prone to error when calculating the stained area. Meanwhile, a very low correlation was

found ($r = -0.23$) between the total stained area and the SIR in the LY site (Fig. 8a). It further demonstrated that much uncertainty remains in assessing the contribution of preferential flow using the dye tracer method. In this study, we did not distinguish the saturated and unsaturated preferential flow. Infiltration under the double-ring is saturated flow, while the tracer front might be unsaturated flow. Whether preferential flow differs substantially under saturated and unsaturated flow conditions might be clarified in the future.

The overall performance of the DI method might be better compared with the dye tracer method. However, it was prone to measurement errors in fields where MI was dominant. As shown in Table 2, the MIR was higher than the SIR at test locations #5 and #7, which was mainly due to the different measurement accuracy of the automatic double-ring infiltrometer and the constant-head infiltrometer. The results of both

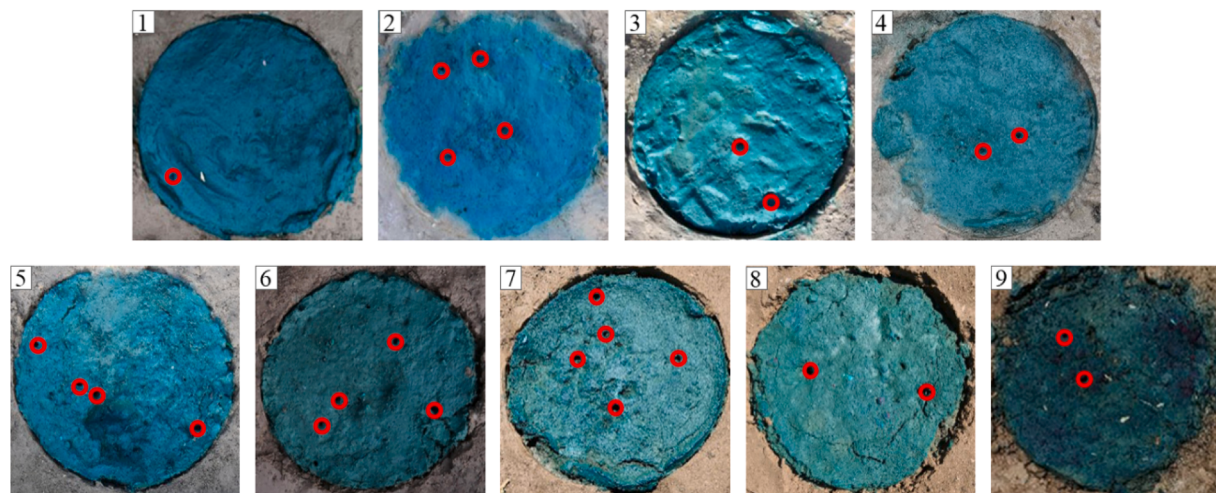


Fig. 7. Distribution of wormholes on the inner ring surface at each test location of the LY site, where red circles are the locations of wormholes. (For interpretation of the references to color in this figure legend, the reader is referred to the web version of this article.)

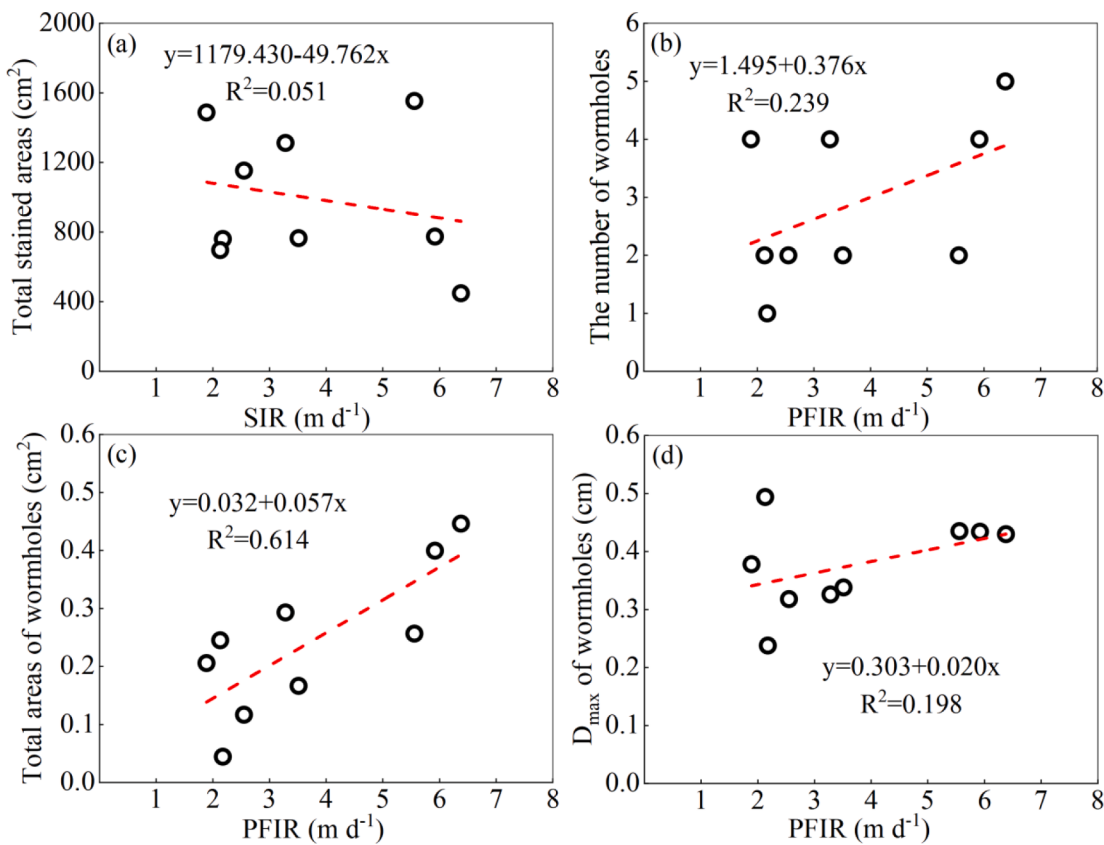


Fig. 8. Results of correlation analysis in the LY site. a) The steady-state infiltration rate (SIR) and total area of the stained soil profile; b) the preferential flow infiltration rate (PFIR) and the number of wormholes; c) the preferential flow infiltration rate (PFIR) and total area of wormholes; d) the preferential flow infiltration rate (PFIR) and maximum diameter (D_{\max}) of wormholes.

Sanders et al. (2012) and Zhang et al. (2019a) demonstrated that infiltration quantification methods in the field are lacking high accuracy. In their studies, they used a double-ring infiltrometer or similar apparatus for measuring soil water infiltration rates, as we did. The size of the ring and the spatial heterogeneity of soils are two major error sources for double-ring infiltrometer (Lai and Ren, 2007; Khodaverdiloo et al., 2017; Bagarello et al., 2021). The future experiments should focus on solving the problem of measurement accuracy of the two instruments.

3.4. Some factors affecting the development of preferential flow

The results of both methods show a relatively large difference in the percentage of preferential flow between the two sites, and the possible reasons for this might be tillage practices and variations in soil texture. As shown in Fig. 5, the Brilliant Blue FCF dye solution could move through the preferential flow channels to a depth of 60 cm in the no-tilled LY site. In contrast, the stained depth of soil profiles was only about 15 cm in the long-term rotary tilled SZ site. The main reason was that tillage disrupted the distribution and connectivity of macropores, which severely affected the occurrence of preferential flow (Bertolino et al., 2010; Wang et al., 2018a). As shown in Table 1, the soil bulk density in the SZ site increased steeply from 1.49 to 1.60 g cm^{-3} at 15 cm. It demonstrated that rotary tillage made the soil top layer looser and the subsoil firmer while leading to the formation of a plow pan in the field. In addition, the presence of the plow pan further limited the vertical infiltration of soil water and increased the potential for lateral infiltration (Jiang et al., 2015).

As shown in Table 1, the sand content of the two sites differed significantly, which most likely influenced the formation of preferential flow. For example, Grant et al. (2019) concluded that preferential flow was more prevalent in clays than in silt loams. Liu et al. (2021) noted

that sandy and clayey soils were prone to macropore and finger flow in their study of the effect of soil properties on preferential flow. One limitation of our method is that we assumed that the only differences between disturbed and undisturbed soils are macropores. This is not a major issue for all horizontal homogeneous soils, but further validation is needed in non-homogeneous soils.

3.5. The relationship between wormholes and PFI

In the LY site, live earthworms could be seen in the macropores of the soil profile and earthworm excreta could be seen on the ground. Therefore, wormholes may be an important factor in the occurrence of preferential flow in this study. To clarify the effect of wormholes on preferential flow, we analyzed the correlation between the number and cross-sectional area of wormholes and the soil infiltration rate. As seen from the field photographs in the LY site, wormholes were present at all test locations (Fig. 7). Of these, test location #7 had the highest number of wormholes, which is five.

As shown in Fig. 8b, the correlation coefficient between the number of wormholes and the PFIR of the LY site was 0.49, which was not significant. However, the results of Zhang et al. (2019b) also showed that saturated hydraulic conductivity was highly positively correlated with the different sizes of macropores. By correlation analysis, the total area of wormholes and the PFIR had a significant correlation, $r = 0.79$, $P < 0.05$ (Fig. 8c). The correlation between the maximum diameter of wormholes and the PFIR of each test location was low, $r = 0.45$ (Fig. 8d). The possible reason is that the size of wormholes in each location was relatively uniform, with a mean diameter of 3.2 ± 0.07 mm. Overall, the total area and number of wormholes affect the soil preferential flow, and further research will need to delve into the effects of other factors such as the length and tortuosity of the wormholes.

The DI method we proposed has the potential to quantify preferential flow, however, the following shortcomings should be overcome to improve the accuracy of preferential flow measurement. First of all, when repacking soil columns, we are not just destroying preferential flow path but we are also might destroy the structure of the soil. The structure of the soil may not always be responsible for the preferential flow, especially for soil with fine textures such as clay or loam. In addition, the DI method includes two different infiltration measurements, which makes the whole experiment and data analysis process a time-consuming task.

4. Conclusion

A new dual infiltration method and dye tracer method were used to quantify the proportion of preferential flow in two sites of North China plain farmland. The results of the dual infiltration method showed that PFI accounted for more than 97% of the SIR in the LY site, while the average contribution in the SZ site was 39%. Results of the dye tracer method indicated that PFI in the LY site was 1.7 times greater than MI, while MI was dominant in the SZ site. The performance of the two methods was analyzed while revealing their sources of error. The dual infiltration method had a promising performance, but the dye tracer method might underestimate the contribution of preferential flow, especially in soil with abundant preferential flow channels. Tillage practices and soil texture may be the important factors affecting preferential flow path development in the two sites. Wormholes played an essential role in the generation of preferential flow in the LY site, and there was a significant correlation between the total area of wormholes and the PFIR ($P < 0.05$). Subsequent studies will consider how to properly quantify the effect of wormholes on preferential flow.

Declaration of Competing Interest

The authors declare that they have no known competing financial interests or personal relationships that could have appeared to influence the work reported in this paper.

Data availability

Data will be made available on request.

Acknowledgments

This research was supported by the Natural Science Foundation of China under Project No. 42077008 and No. 41771257. Our deepest gratitude went to the anonymous reviewers for their careful work and thoughtful suggestions that have helped us to improve this paper.

References

- Abou Najm, M.R., Jabro, J.D., Iversen, W.M., Mohtar, R.H., Evans, R.G., 2010. New method for the characterization of three-dimensional preferential flow paths in the field. *Water Resour. Res.* 46, W02503.
- Alaoui, A., 2015. Modeling susceptibility of grassland soil to macropore flow. *J. Hydrol.* 525, 536–546.
- Alaoui, A., Goetz, B., 2008. Dye tracer and infiltration experiments to investigate macropore flow. *Geoderma* 144, 279–286.
- Ankeny, M.D., Ahmed, M., Kasper, T.C., Horton, R., 1991. A simple field method for determining unsaturated hydraulic conductivity. *Soil Sci. Soc. Am. J.* 55, 467–470.
- Arrington, K.E., Ventura, S.J., Norman, J.M., 2013. Predicting saturated hydraulic conductivity for estimating maximum soil infiltration rates. *Soil Sci. Soc. Am. J.* 77 (3), 748–758.
- Bagarello, V., Sferlazza, S., Sgroi, A., 2009. Comparing two methods of analysis of single-ring infiltrometer data for a sandy-loam soil. *Geoderma* 149 (3–4), 415–420.
- Bagarello, V., Barca, E., Castellini, M., Iovino, M., Morbidelli, R., Saltalippi, C., Flammini, A., 2021. A plot-scale uncertainty analysis of saturated hydraulic conductivity of a clay soil. *J. Hydrol.* 596, 125694.
- Benegas, L., Ilstedt, U., Roupsard, O., Jones, J., Malmer, A., 2014. Effects of trees on infiltrability and preferential flow in two contrasting agroecosystems in Central America. *Agric. Ecosyst. Environ.* 183, 185–196.
- Bertolino, A.V.F.A., Fernandes, N.F., Miranda, J.P.L., Souza, A.P., Lopes, M.R.S., Palmieri, F., 2010. Effects of plough pan development on surface hydrology and on soil physical properties in Southeastern Brazilian plateau. *J. Hydrol.* 393 (1), 94–104.
- Beven, K., Germann, P., 2013. Macropores and water flow in soils revisited. *Water Resour. Res.* 49, 3071–3092.
- Bouwer, H., 1986. Intake rate: cylinder infiltrometer. In: A. Klute (ed.), *Methods of Soil Analysis, Part 1*, ASA Monograph No. 5, Madison, WI.
- Cey, E.E., Rudolph, D.L., 2009. Field study of macropore flow processes using tension infiltration of a dye tracer in partially saturated soils. *Hydrol. Process.* 23 (12), 1768–1779.
- Ferreira, T., Rasband, W., 2012. ImageJ User Guide, IJ (1.46r, revised edition).
- Filipović, V., Deffterdarović, J., Šimunek, J., Filipović, L., Ondrášek, G., Romić, D., Bogunović, I., Mustać, I., Čurić, J., Kodešová, R., 2020. Estimation of vineyard soil structure and preferential flow using dye tracer, X-ray tomography, and numerical simulations. *Geoderma* 380, 114699.
- Flury, M., Flühler, H., 1995. Tracer characteristics of brilliant blue FCF. *Soil Sci. Soc. Am. J.* 59, 22–27.
- Germann-Heins, J., Flury, M., 2000. Sorption of Brilliant Blue FCF in soils as affected by pH and ionic strength. *Geoderma* 97, 87–101.
- Germann, P.F., Beven, K., 1985. Kinematic wave approximation to infiltration into soils with sorbing macropores. *Water Resour. Res.* 21 (7), 990–996.
- Grant, K.N., Macrae, M.L., Ali, G.A., 2019. Differences in preferential flow with antecedent moisture conditions and soil texture: Implications for subsurface P transport. *Hydrol. Process.* 33 (15), 2068–2079.
- Greve, A., Andersen, M.S., Aworth, R.I., 2010. Investigations of soil cracking and preferential flow in a weighing lysimeter filled with cracking clay soil. *J. Hydrol.* 393 (1), 105–113.
- Grossman, R.B., Reinsch, T.G., 2002. Bulk density and linear extensibility. In: J.H. Dane, C.G. Topp, editors, *Methods of soil analysis, Part 4*. SSSA Book Ser. 5.4. SSSA, Madison, WI.
- Guo, L., Lin, H., 2018. Addressing two bottlenecks to advance the understanding of preferential flow in soils. *Adv. Agron.* 147, 61–117.
- Hill, D.E., Parlange, J.-Y., 1972. Wetting front instability in layered soils. *Soil Sci. Soc. Am. J.* 36 (5), 697–702.
- Jiang, X.J., Liu, X.E., Wang, E.H., Li, X.G., Sun, R., Shi, W.J., 2015. Effects of tillage pan on soil water distribution in alfalfa-corn crop rotation systems using a dye tracer and geostatistical methods. *Soil Till. Res.* 150, 68–77.
- Khodaverdiloo, H., Cheraghbal, H.K., Bagarello, V., Iovino, M., Asgarzadeh, H., Dashtaki, S.G., 2017. Ring diameter effects on determination of field-saturated hydraulic conductivity of different loam soils. *Geoderma* 303, 60–69.
- Kianpoor Kalkhajeh, Y., Huang, B., Hu, W., 2021. Impact of preferential flow pathways on phosphorus leaching from typical plastic shed vegetable production soils of China. *Agric. Ecosyst. Environ.* 307.
- Klute, A., Dirksen, A., 1986. Hydraulic conductivity and diffusivity: Laboratory methods. In: A. Klute, (ed.), *Methods of Soil Analysis, Part 1*, ASA Monograph No. 9, Madison, WI.
- Kodešová, R., Němcék, K., Kodeš, V., Žigová, A., 2012. Using dye tracer for visualization of preferential flow at macro- and microscales. *Vadose Zone J.* 11 (1).
- Kodešová, R., Němcék, K., Žigová, A., Nikodem, A., Féral, M., 2015. Using dye tracer for visualizing roots impact on soil structure and soil porous system. *Biology* 70 (11), 1439–1443.
- Lai, J.B., Ren, L., 2007. Assessing the size dependency of measured hydraulic conductivity using double-ring infiltrometers and numerical simulation. *Soil Sci. Soc. Am. J.* 71 (6), 1667–1675.
- Laine-Kaulio, H., Backnäs, S., Koivusalto, H., Laurén, A., 2015. Dye tracer visualization of flow patterns and pathways in glacial sandy till at a boreal forest hillslope. *Geoderma* 259, 23–34.
- Liu, Y., Zhang, Y., Xie, L., Zhao, S., Dai, L., Zhang, Z., 2021. Effect of soil characteristics on preferential flow of Phragmites australis community in Yellow River delta. *Ecol. Indic.* 125.
- Marquart, A., Goldbach, L., Blaum, N., 2020. Soil-texture affects the influence of termite macropores on soil water infiltration in a semi-arid savanna. *Ecohydrology* 13 (8), e2249.
- Marshall, T.J., Holmes, J.W., Rose, C.W., 1996. *Soil Physics*, third ed. Cambridge University Press, New York.
- Mei, X., Zhu, Q., Ma, L., Zhang, D., Wang, Y., Hao, W., 2018. Effect of stand origin and slope position on infiltration pattern and preferential flow on a loess hillslope. *Land Degrad. Dev.* 29, 1353–1365.
- Moberly, J.G., Bernards, M.T., Waynant, K.V., 2018. Key features and updates for Origin 2018. *J. Cheminform.* 10 (1).
- Mohanty, B.P., Horton, R., Ankeny, M.D., 1996. Infiltration and macroporosity under a row crop agricultural field in a glacial till field. *Soil Sci.* 161, 205–213.
- Nobles, M.M., Wilding, L.P., Lin, H.S., 2010. Flow pathways of bromide and Brilliant Blue FCF tracers in caliche soils. *J. Hydrol.* 393 (1–2), 114–122.
- Philip, J.R., 1957. The theory of infiltration: 4. Sorptivity and algebraic infiltration equations. *Soil Sci.* 84, 257–264.
- Salvador, M.M.S., Köhne, S., Köhne, J.M., Lennartz, B., Libardi, P.L., 2011. Dye tracer and morphophysical properties to observe water flow in a Gleyic Luvisol. *Sci. Agr.* 68 (2), 160–166.
- Sander, T., Gerke, H.H., 2007. Preferential flow patterns in paddy fields using a dye tracer. *Vadose Zone J.* 6, 105–115.
- Sanders, E.C., Abou Najm, M.R., Mohtar, R.H., Kladivko, E., Schulze, D., 2012. Field method for separating the contribution of surface-connected preferential flow pathways from flow through the soil matrix. *Water Resour. Res.* 48 (4), 1427–1434.

- Schwen, A., Backus, J., Yang, Y., Wendoroth, O., 2014. Characterizing land use impact on multi-tracer displacement and soil structure. *J. Hydrol.* 519, 1752–1768.
- Shukla, M.K., 2013. Soil Physics: An Introduction. CRC Press, Taylor & Francis Group.
- Stewart, R.D., Abou Najm, M.R., Rupp, D.E., Lane, J.W., Uribe, H.C., Arumí, J.L., Selker, J.S., 2015. Hillslope run-off thresholds with shrink-swell clay soils. *Hydrology Process.* 29 (4), 557–571.
- Stewart, R.D., Abou Najm, M.R., Rupp, D.E., Selker, J.S., 2016. Modeling multidomain hydraulic properties of shrink-swell soils. *Water Resour. Res.* 52 (10), 7911–7930.
- Stumpff, C., Maloszewski, P., 2010. Quantification of preferential flow and flow heterogeneities in an unsaturated soil planted with different crops using the environmental isotope $\delta^{18}\text{O}$. *J. Hydrol.* 394, 407–415.
- Sun, Q., Zhang, J.F., Zhang, J., Zeng, H., Hu, K.L., Liu, G., 2020. Design and experiment of automatic double-ring infiltrometer. *Trans. Chin. Soc. Agric. Eng.* 36 (10), 318–324.
- Surajit, D.G., Mohanty, B.P., Köhne, J.M., 2006. Soil hydraulic conductivities and their spatial and temporal variations in a vertisol. *Soil Sci. Soc. Am. J.* 70 (6), 1872–1881.
- Svensson, D.N., Messing, I., Barron, J., 2022. An investigation in laser diffraction soil particle size distribution analysis to obtain compatible results with sieve and pipette method. *Soil Till. Res.* 223, 105450.
- Tobella, A.B., Reese, H., Almaw, A., Bayala, J., Malmer, A., Laudon, H., Ilstedt, U., 2014. The effect of trees on preferential flow and soil infiltrability in an agroforestry parkland in semiarid Burkina Faso. *Water Resour. Res.* 50 (4), 3342–3354.
- van Schaik, N.L.M.B., 2009. Spatial variability of infiltration patterns related to site characteristics in a semi-arid watershed. *Catena* 78 (1), 36–47.
- van Schaik, N.L.M.B., Hendriks, R.F.A., van Dam, J.C., 2010. Parameterization of macropore flow using dye-tracer infiltration patterns in the SWAP model. *Vadose Zone J.* 9 (1).
- Wang, F., Chen, H.S., Lian, J.J., Fu, Z.Y., Nie, Y.P., 2018a. Preferential flow in different soil architectures of a small karst catchment. *Vadose Zone J.* 17 (1), 180107.
- Wang, Y., Wang, X., Chau, H.W., Si, B.C., Yao, N., Li, Y., 2018b. Water movement and finger flow characterization in homogenous water-repellent soils. *Vadose Zone J.* 17 (1), 180021.
- Wu, G.L., Cui, Z., Huang, Z., 2021. Contribution of root decay process on soil infiltration capacity and soil water replenishment of planted forestland in semi-arid regions. *Geoderma* 404, 115289.
- Wu, Q.H., Liu, C.L., Lin, W.J., Zhang, M., Wang, G.L., Zhang, F.W., 2015. Quantifying the preferential flow by dye tracer in the North China Plain. *J. Earth Sci-China* 26 (3), 435–444.
- Wu, L., Pan, L., Roberson, M.J., Shouse, P.J., 1997. Numerical evaluation of ring-infiltrometers under various soil conditions. *Soil Sci.* 162 (11), 771–777.
- Zeleke, T.B., Si, B.C., 2005. Scaling relationships between saturated hydraulic conductivity and soil physical properties. *Soil Sci. Soc. Am. J.* 69 (6), 1691–1702.
- Zhang, J., Lei, T.W., Qu, L.Q., Chen, P., Gao, X.F., Chen, C., Yuan, L.L., Zhang, M.L., Su, G.X., 2017. Method to measure soil matrix infiltration in forest soil. *J. Hydrol.* 552, 241–248.
- Zhang, J., Lei, T.W., Qu, L.Q., Zhang, M.L., Chen, P., Gao, X.F., Chen, C., Yuan, L.L., 2019a. Method to quantitatively partition the temporal preferential flow and matrix infiltration in forest soil. *Geoderma* 347, 150–159.
- Zhang, X., Zhu, J.F., Wendoroth, O., Matocha, C., Edwards, D., 2019b. Effect of macroporosity on pedotransfer function estimates at the field scale. *Vadose Zone J.* 18, 180151.
- Zhu, X.A., Chen, C.F., Wu, J.E., Yang, J.B., Zhang, W.J., Zou, X., Liu, W.J., Jiang, X.J., 2019. Can intercrops improve soil water infiltrability and preferential flow in rubber-based agroforestry system? *Soil Till. Res.* 191, 327–339.